TECHNISCHE MECHANIK, 32, 2-5, (2012), 155 – 163
submitted: November 1, 2011

Modeling Tube-Forming of an Austenitic Stainless Steel with Exploitation of Martensite Evolution

T. Dally, C. Müller-Bollenhagen, H.-J. Christ, K. Weinberg

Within the last years the industrial manufacturing of tubes has developed to an increasingly complex process. In particular, during the forming procedure of sheets made of austenitic stainless steel, the increase and the content of strain-induced martensite needs to be controlled in order to achieve the optimal structural properties of the manufactured tube with respect to very-high-cycle fatigue (VHCF). On the basis of experimental investigations this contribution deals with the numerical simulation of the forming process with special consideration of the martensite ratio as a function of temperature and deformation field. A convenient approach of modeling the martensite evolution as well as the extension of this model to polyaxial states of stress and a comparison with experimental results is presented.

1 Technological Background

Within the last decade engineers became more and more aware of the fact that a given high cycle fatigue may not be sufficient to guarantee reliability of certain machine components. Structures like engine parts, train wheels, rotors, medical devices or offshore components often have to sustain high frequency vibrations and thus a number of life cycles much higher than 10^6. The need for a long life expectation of such components has raised interest in investigating materials in the very high cycle fatigue (VHCF) regime, i.e., with loading cycles of $10^7 \ldots 10^{10}$. Especially for metastable austenitic steel it appeared that there is a certain volume fraction of martensite which optimizes the resistance to VHCF. Therefore, we present in this contribution a strategy to model and numerically simulate the evolution of martensite in a metastable steel sheet, which can be employed to control process parameters during industrial forming.

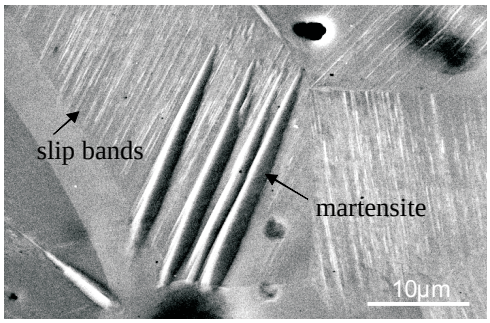

Figure 1: Needles of martensite in X5CrNi18-10 steel after after 10^9 cycles

The mechanical properties of austenitic stainless steel are known to significantly improve with growing martensite content. For example, the transformation induced lattice change from face-centered cubic γ-austenite to body-centered cubic α'-martensite increases the dislocation density in the austenitic phase which, in turn, raises its strength. Moreover, martensite works as a barrier against microscopic crack growth and, thus, the material resistance is increased. Figure 1 displays the microstructure of a specimen after cycling in the VHCF regime (10^9 cycles with a stress amplitude of 245 MPa); the VHCF fatigue properties are strongly influenced by the formation of slip bands and martensite needles.

In material science there exist a wide range of models that describe the martensite evolution during plastic deformation of metastable austenitic steel. However, many of these models are rather simple and do not even account for the influence of a temperature change while deformation and for the strain rate sensitivity of the martensite

formation, cf. Müller-Bollenhagen (2011) for a review. A classical model was introduced by Olson and Cohen (1975) who suggest a direct dependence between the formation of martensite embryos and the quantity of shear band crossings; therefore facilitating a calculation of the martensite ratio as a function of strain. Stringfellow et al. (1992) modified this early model in such a manner that also the stress-state of the material was regarded as a component for the martensite evolution. Tomita and Iwamoto (1995) presented another modification based on experimental observations and stated an influence of the strain rate on the formation of shear bands. Another martensite model was developed by Tsuta and Cortes (1993) who suggested a polynomial function which needs to be calibrated against tension tests. This model was modified and formulated incrementally by Heinemann (2004) and Springub (2006). Most of these macroscopic models described the martensite evolution as a function of temperature and strain in an uniaxial way. However, here we consider a stepwise forming process which requires a model applicable to multi-axial states. Beside temperature, stress-state and strain there are moreover additional influencing factors for the evolution of martensite. Waitz et al. (2009) found out that the formation of thermally induced martensite strongly depends on the grain size of the material and can be completely suppressed if the grain size is too small. Of course the martensite evolution is crucially influenced by the material's composition; for example a high carbon concentration obstructs the martensite evolution, cf. Krupp and Christ (2008).

The formation of martensite corresponds to a high amount of shear bands and shear band crossings and requires a particulary high local shear stress in the grain. The ratios of shear stress in the local slip plane to the applied external tension (Schmid factors) visualized by means of Electron Backscatter Diffraction (EBSD) scans are depicted in Figure 2. The displayed specimen have been prestrained ($\varepsilon = 0.15$) in order to reach 20 vol.% of martensite. Subsequently they are loaded in two different ways. For a specimen pulled again in the same horizontal direction the Schmid factors of different grains are shown in Figure 2 a); the white areas are martensitic. Clearly, martensite forms in areas with high Schmid factors which correlates to a high density of shear bands. Figure 2 b) shows the Schmid factors for the same specimen now pulled in orthogonal direction. Again, grains with a high Schmid factor will deform plastically. However, the Schmid factor in grains with accumulated martensite is now reduced. This indicates that not only the total strain but also its direction influence the amount of martensite following from a certain shear band volume fraction. We will quantify this effect in our martensite formation model.

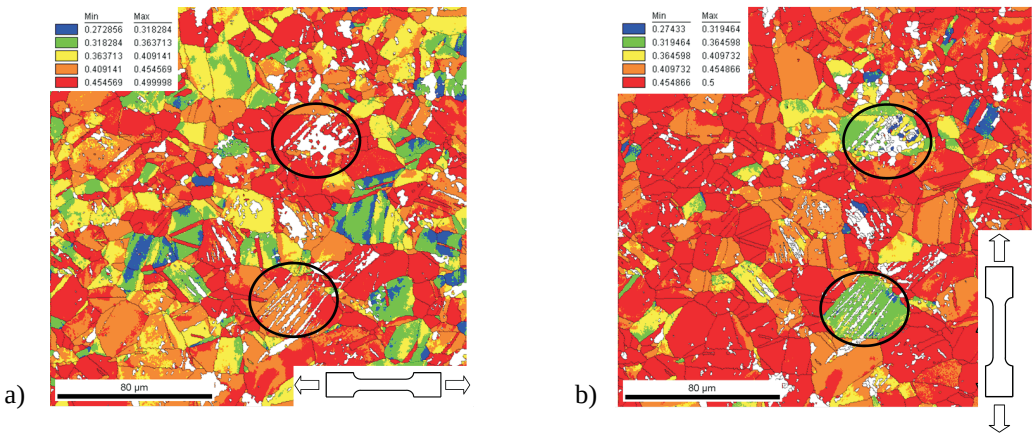

Figure 2: Schmid factors in tensile specimens of 20 vol.% martensite in uniaxial and two-axial deformation (blue: minimum, red: maximum, white: martensite)

The remaining of the paper is organized as follows: In the next section we describe the concept of VHCF testing and provide investigations of the VHCF properties of X5CrNi18-10 steel. Then, in Section 3, we shortly introduce the underlying continuum mechanical model and present an approach to calculate the rate of martensite evolution. A discussion of the model is also given in Section 3. The last section summarizes our numerical results and presents the application of our model in a forming simulation of metastable X5CrNi18-10 steel sheets.

2 Resistance to VHCF

In the literature the VHCF-behavior of metallic materials is often classified in type I materials (ductile single phase materials without intrinsic defects) and type II materials (high strength steels with intrinsic defects). Surface roughening caused by local plastic deformation in favorably oriented grains is seen as the predominant damage mechanism in VHCF regime for type I materials. In contrast, type II materials often show local plastic deformation at inclusions that can lead to crack initiation due to debonding of the inclusion-matrix interface or breaking of non-

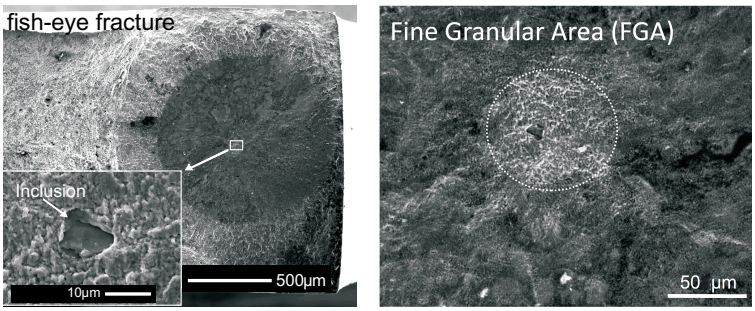

Figure 3: Modes of VHCF failure: fish-eye fracture along inclusions in a specimen of 27 vol.% of martensite (left) and failure by fine granular area in a specimen of 54 vol.% of martensite (right)

metallic inclusions. Because of their high ductility austenitic stainless steels may be categorized as type I materials regarding the VHCF-behavior. However, metastable steels like X5CrNi18-10 undergo a deformation-induced phase transformation from austenite to ε-martensite and to the hard α'-martensite phase. This phenomenon of transformation induced plasticity enables excellent strength and ductility and has been investigated intensively, for example by Fischer et al. (2000) and Dimatteo et al. (2006). Moreover, they show a pronounced strain hardening and can contain different types of inclusions. These properties classify X5CrNi18-10 for the type II category. However, our experimental observations showed that in particular in clusters of martensite the dominant failure mode in the VHCF regime changes from surface roughening (Figure 1) to internal crack initiation leading to fish-eye fracture. A very slow crack propagation starting from inclusions is the reason for a Fine Granular Area (FGA), see Figure 3. This Fine Granular Area fracture was found to be particulary dominant at a high martensite content.

In order to develop a quantitative relationship between the volume fraction of martensite and the VHCF behavior several specimens were monotonically prestrained in two different ways and compared to virgin austenitic specimen. Firstly, a one-step plastic deformation at different temperatures resulting in two martensite volume contents (27% and 54%) and secondly, a two-step deformation by constant temperature but different amounts of deformation in order to reach the 27% and the 54% of martensite volume were performed. The latter deformation leads to a higher dislocation density. The results of the VHCF tests are displayed in Figure 4 and 5.

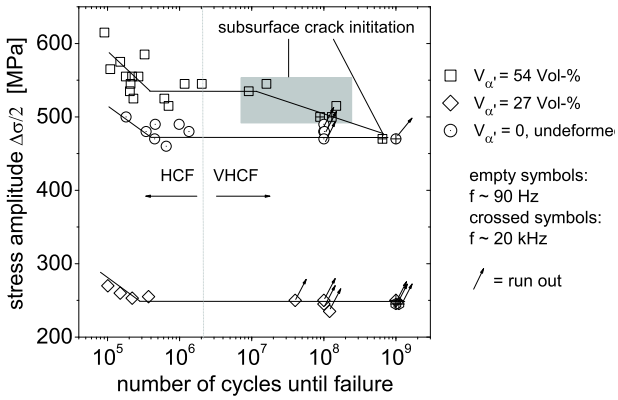

Figure 4: S-N curves for one-step deformed specimens with different martensite content

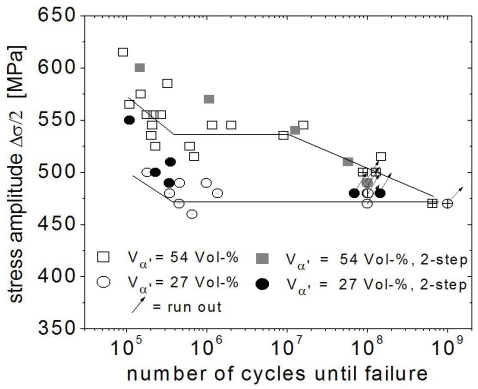

Figure 5: S-N curves for two-step predeformed specimens with different martensite content

In the fully austenitic condition a true VHCF fatigue limit exists. The constant fatigue limit is mainly caused by a martensite-assisted cyclic hardening process. A higher martensite content of 27 vol % martensite enhances the HCF properties and the fatigue limit remains independent of the number of cycles even in the VHCF regime. At 54 vol.% martensite the more brittle behavior of the martensite phase enables crack initiation at inclusions and the formation of FGAs leading to failure in the VHCF regime.
Figure 5 shows the VHCF fatigue limit of the two-step predeformed specimens which has the same gradient as the one-step limit for 54 vol.%. The two-step deformed specimens with 27 vol.% martensite also showed a behavior similar to the one-step deformed counterparts, even though the yield strength and dislocation density of these specimen were considerably higher. The VHCF properties are not determined by dislocation density and direction or amount of predeformation but by the martensite content instead. These and further experimental observations

lead us to conclude that a volume fraction of 25-30 vol.% of martensite is required for optimal VHCF resistance of this steel.

3 Mechanical Modeling of Martensite Formulation

3.1 Continuummechanical Model of Metastable CrNi Steel

The state of motion of a solid is fully described by the deformation gradient $\boldsymbol{F}$ which can be divided into an elastic and a plastic component, $\boldsymbol{F} = \boldsymbol{F}^e \boldsymbol{F}^p$. This multiplicative split leads to the following representation of the spatial velocity gradient,

$$\boldsymbol{l} = \dot{\boldsymbol{F}}\boldsymbol{F}^{-1} = \underbrace{\dot{\boldsymbol{F}}^e (\boldsymbol{F}^e)^{-1}}_{=:\boldsymbol{l}^e} + \boldsymbol{F}^e \underbrace{\dot{\boldsymbol{F}}^p (\boldsymbol{F}^p)^{-1}}_{=:\boldsymbol{l}^p} (\boldsymbol{F}^e)^{-1} \ ,$$

which will be linearized as indicated. The considered material is now characterized by a free Helmholtz-energy-density

$$A = A(\boldsymbol{F}^e, \boldsymbol{F}^p, \varepsilon^p, T)$$

with effective plastic strain ε^p and temperature T. The rate of plastic deformation is subjected to the von Mises-flow rule

$$\boldsymbol{l}^p = \dot{\varepsilon^p}\boldsymbol{M} \ \text{ with tr}\,(\boldsymbol{M}) = 0, \ \ \boldsymbol{M} \cdot \boldsymbol{M} = \frac{3}{2}, \ \ \dot{\varepsilon}^p \geq 0,$$

where tensor $\boldsymbol{M}$ describes the direction of plastic flow. Now the free Helmholtz-energy-density can be splitted into an elastic and a plastic part which again is additively decomposed into work hardening and phase transforming components (a more detailed description is given in Dally and Weinberg (2011)):

$$A = W^e(\varepsilon^e, T) + W^p(\varepsilon^p, T) = W^e(\varepsilon^e, T) + W^\gamma(\varepsilon^p, T) + W^{\alpha'}(\varepsilon^p, T).$$

In an time-incremental approach with $\Delta t = t_{n+1} - t_n$ this energy will be optimized with respect to the plastic variables. The used constitutive update algorithm starts with the assumption that the material's state at time t_n and the state of deformation and temperature at time t_{n+1} is given. The problem is to determine the state of the material at time t_{n+1}. For this purpose an incremental deformation energy function f_n is formulated:

$$f_n(\boldsymbol{\varepsilon}_{n+1}, T_{n+1}, \varepsilon^p_{n+1}, \boldsymbol{M}) = W^e(\varepsilon^e_{n+1}, T_{n+1}) + W^\gamma(\varepsilon^p_{n+1}, T_{n+1}) + W^{\alpha'}(\varepsilon^p_{n+1}, T_{n+1}).$$

Minimization of f_n with respect to the inner variables leads to the effective incremental strain-energy density:

$$W_{\text{eff}}(\boldsymbol{\varepsilon}_{n+1}, T_{n+1}) = \min_{\varepsilon^p_{n+1}, \boldsymbol{M}} f_n(\boldsymbol{\varepsilon}_{n+1}, T_{n+1}, \varepsilon^p_{n+1}, \boldsymbol{M}).$$

The definition of an elastic predictor strain $\boldsymbol{\varepsilon}^{\text{trial}}_{n+1} = \boldsymbol{\varepsilon}_{n+1} - \boldsymbol{\varepsilon}^p_n$ and the according trial stress $\boldsymbol{\sigma}^{\text{trial}}_{n+1} = 2\mu\boldsymbol{\varepsilon}^{\text{trial, dev}}_{n+1}$ facilitates the following restatement of f_n:

$$f_n(\boldsymbol{\varepsilon}_{n+1}, T_{n+1}, \varepsilon^p_{n+1}, \boldsymbol{M}) = W^e(\boldsymbol{\varepsilon}^{\text{trial}}_{n+1} - \Delta\boldsymbol{\varepsilon}^p \boldsymbol{M}_{n+1}, T_{n+1}) + W^p(\varepsilon^p_{n+1}, T_{n+1}).$$

The effective plastic strain ε^p_{n+1} then can be evaluated by solving

$$\left|\left|\boldsymbol{\sigma}^{\text{trial}}_{n+1} - 3\mu\Delta\varepsilon^p \frac{\boldsymbol{\sigma}^{\text{trial}}_{n+1}}{||\boldsymbol{\sigma}^{\text{trial}}_{n+1}||}\right|\right| - \sigma_0 \left(1 + \frac{\varepsilon^p_n + \Delta\varepsilon^p}{\varepsilon_0}\right)^{\frac{1}{m}} - \sigma_0 \left(\frac{\dot{\varepsilon}^p}{\dot{\varepsilon}^p_0}\right)^{\frac{1}{k}} = 0 \tag{1}$$

using a Newton-Raphson iteration. Here $\sigma_0 = \sigma_0(T)$ is the initial yield stress and m the hardening exponent. Aside of the last term which follows from martensite hardening, Equation (1) corresponds to classical von Mises plasticity.

3.2 Evolution of Martensite

The assumption that the formation of martensite during forming processes strongly depends on the temperature is supported by specific experiments: The left picture in Figure 6 shows the martensite formation in a specimen which is strained uniaxially with $\varepsilon = 0.14$ at a starting temperature of $T(0) = -70°\text{C}$. In the middle picture the tension test is progressed with $\varepsilon = 0.34$ at ambient temperature $T(0) = 23°\text{C}$. Both experiments lead to a similar martensite ratio of $c \approx 0.55$ in the specimens - however the arrangements of the martensitic sections differ from

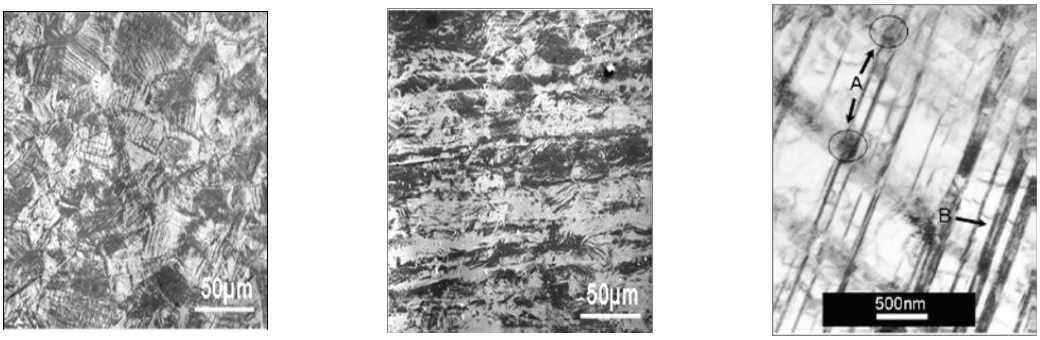

Figure 6: Formation of martensite (dark areas) in austenitic steel; specimen uniaxially strained with $\epsilon = 0.15$ at $T = -70^oC$ (left) and $\epsilon = 0.34$ at $T = -70^oC$ (middle), both resulting in approximately 54 vol.% martensite. At right the martensite fraction is 25 vol.%, here shear band crossings (A) and shear bands (B) are marked.

each other. In the right picture the martensite formation is illustrated for a specimen which is strained uniaxially with $\varepsilon = 0.15$ at a starting temperature of $T(0) = -20°\mathrm{C}$. The shear bands and shear band crossings which work as seeding points for martensite evolution are indicated.

Experimental observations suggest a direct dependence between the formation of martensite embryos and the quantity of shear band crossings which can be determined by the shear band volume. Therefore, our point of departure to model the martensite evolution is the classical model of Olson and Cohen (1975). In incremental form it reads

$$\begin{aligned} \frac{\partial c}{\partial \varepsilon} &= \alpha\, n\, \beta\, s^{n-1}(1-s)(1-c)\,, \\ \frac{\partial s}{\partial \varepsilon} &= \alpha\,(1-s), \end{aligned} \tag{2}$$

with martensite ratio c and strain ε, whereas α denotes the rate of shear band evolution, β is the probability of martensite formation at a shear band crossing, s the ratio of shear band volume and n is a material specific constant. In the original model α and β are assumed to be constant during the simulation with the result, that the model is only applicable for isothermal processes. However, due to the fact that the temperature T changes rapidly during the regarded processes like tension tests or sheet forming, a non-isothermal evolution equation for martensite formation is required.

For this purpose we extend the model of Olson and Cohen (1975) in such a manner that we set the constants α and β as functions of temperature and current martensite ratio:

$$\begin{aligned} \alpha(T) &= \alpha_1 \cdot T^{\alpha_2}, \\ \beta(T,c) &= \beta_1 \cdot \exp\left(\beta_2\, T + \beta_3\, c\right), \end{aligned}$$

with constants $\alpha_1, \alpha_2, \beta_1, \beta_2$ and β_3, which need to be adjusted to the specific material. This corresponding adjustment takes into account that the martensite evolution depends on the grain size (see Waitz et al. (2009)). An extension of this non-isothermal but uniaxial model to polyaxial states of stress is outlined in the following.

Let us first consider a sheet which is deformed in one direction $\mathbf{x}$ and afterwards in an orthogonal direction $\mathbf{y}$ with the amounts ε_x and ε_y respectively, see Figure 7. From experimental observations it is known that only a certain ratio Ψ of the composed shear bands in $\mathbf{x}$-direction is significant concerning the martensite evolution in $\mathbf{y}$-direction. In the following c_x and c_y denote the martensite rates and s_x, s_y the rates of shear band volumes which are induced by the strains ε_x and ε_y. In order to calculate the martensite ratio in such a biaxial tension test one has to calculate s_x, s_y and c_x using equation (2). At the calculation of c_y, however, one has to add the relevant part $\Psi \cdot s_x$ of the shear band volume ratio composed in $\mathbf{x}$-direction additionally to s_y :

$$\frac{\partial c_y}{\partial \varepsilon_y} = \alpha\, n\, \beta\, (s_y + \Psi \cdot s_x)^{n-1}(1 - (s_y + \Psi \cdot s_x))(1 - c_y).$$

Finally the martensite rates c_x and c_y based on the strains ε_x and ε_y get combined, see Figure 9, so that the total martensite ratio of

$$c = c_x + (1 - c_x) \cdot c_y = c_x + c_y - c_x c_y$$

is obtained. A similar procedure is applicable in the case of a sheet that is pulled in three spatial directions by the eigenstrains $\varepsilon_1, \varepsilon_2$ and ε_3: For $i, I = 1, 2, 3$ (no summation) the martensite ratios c_i induced by ε_I is calculated by

$$\frac{\partial c_i}{\partial \varepsilon_I} = \alpha\, n\, \beta\, (s_i + \Psi \cdot \sum_{j=1, j\neq i}^{3} s_j)^{n-1} (1 - (s_i + \Psi \cdot \sum_{j=1, j\neq i}^{3} s_j))(1 - c_i)$$

and their combination gives

$$c = c_1 + (1 - c_1) \cdot c_2 + (1 - c_1 - (1 - c_1) \cdot c_2) \cdot c_3 = c_1 + c_2 + c_3 - c_1 c_2 - c_1 c_3 - c_2 c_3 + c_1 c_2 c_3.$$

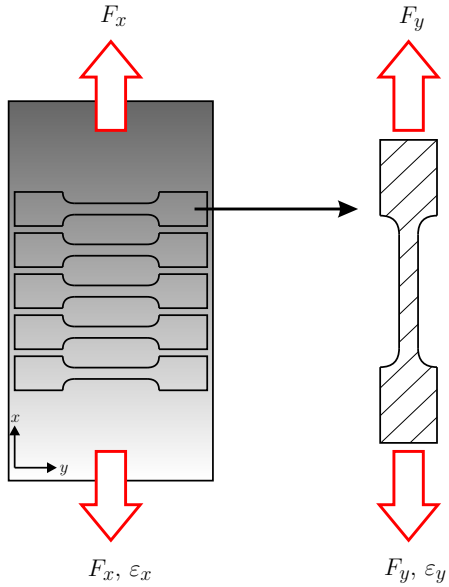

Figure 7: Two-directional tension test. The specimen is first deformed in $\boldsymbol{x}$-direction, afterwards in orthogonal $\boldsymbol{y}$-direction

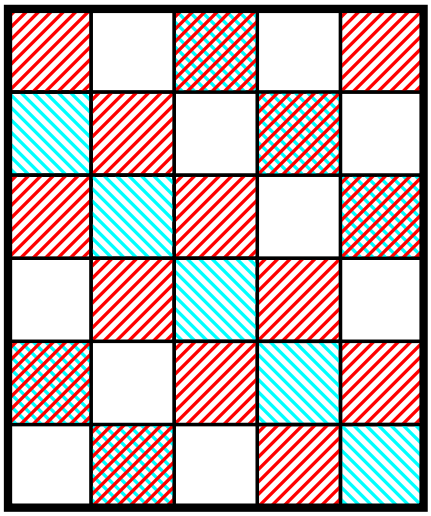

Figure 8: Combination of martensite ratios c_x and c_y to the total martensite ratio c

4 Simulation Results

4.1 Tensile Tests

At first we study the martensite evolution at uni-directional and two-directional tension tests. Figure 9 shows the increase of the martensite ratio for different initial temperatures $T(0)$ and exposes the support of martensite evolution by low temperatures. In Figure 10 the martensite ratio depending on the strain rate $\dot{\varepsilon}$ is presented. It becomes obvious that the martensite evolution is inhibited due to low heat emission if a high strain rate is applied. The nice correlation between the simulations and the experimental results marked by dashed lines in both Figures becomes obvious.

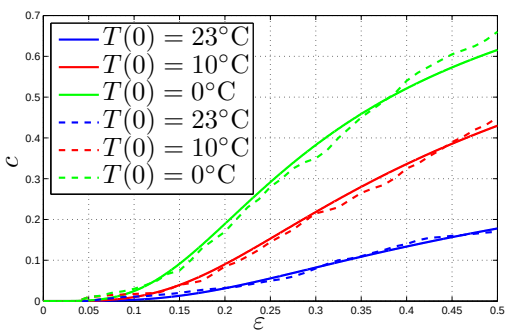

Figure 9: Martensite volume fraction c as a function of ε and $T(0)$; $\dot{\varepsilon} = 0.005 s^{-1}$

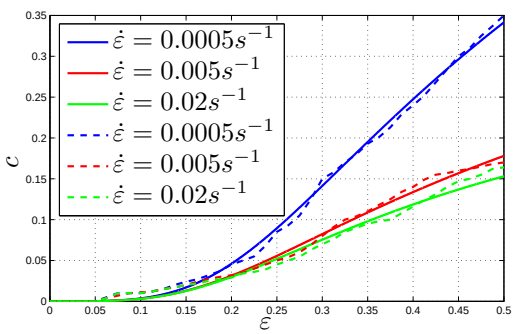

Figure 10: Martensite volume fraction c as a function of ε and $\dot{\varepsilon}$; $T(0) = 23°C$

Now we consider a specimen that is deformed in one direction $\mathbf{x}$ with $\varepsilon_x = \frac{1}{4}$ in the first stage followed by a deformation in an orthogonal direction $\mathbf{y}$ with $\varepsilon_y = \frac{1}{4}$. In Figure 11 the martensite evolution is illustrated by using a strain rate of $\dot{\varepsilon} = 0.0005s^{-1}$ during the first, but different strain rates during the second stage of the forming process. The best correlation between experimental data (again marked by dashed lines) and simulation results is performed with $\Psi \approx 3/4$. In Figure 12 the martensite evolution is presented for different initial temperatures. The progression of c is similar but not identical to the one during the uniaxial tension test presented in Figure 9. (In both Figures the first derivative of c is discontinuous at $\varepsilon = 0.25$ due to the change of loading direction.)

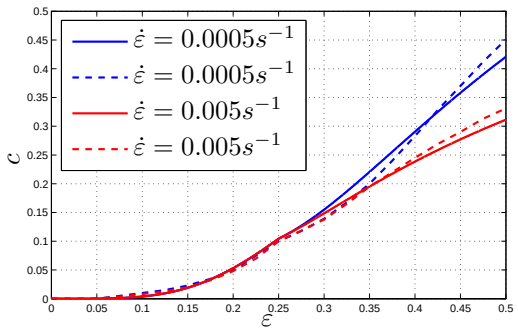

Figure 11: Martensite volume fraction c as a function of ε and $\dot{\varepsilon}$; $T(0) = 23°\mathrm{C}$, $\Psi = 0.75$, $\dot{\varepsilon} = 0.0005s^{-1}$, first stage of forming

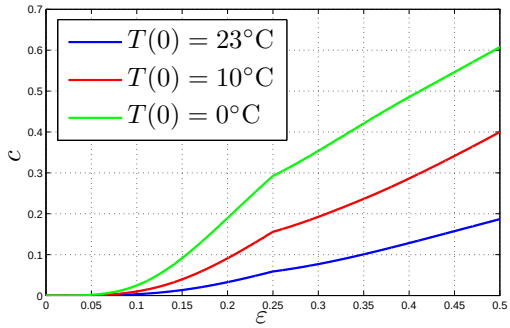

Figure 12: Martensite volume fraction c as a function of ε and $T(0)$; $\dot{\varepsilon} = 0.005s^{-1}$, $\Psi = 0.75$

4.2 Forming Simulation of an X5CrNi18-10 Sheet

Finally we have a closer look on the local martensite evolution during a process that forms a X5CrNi18-10-sheet to a tube. One possibility of forming such a tube is presented in Figure 13: At first a sheet made of austenitic stainless steel is transformed by corresponding tools and welded to a conventional tube. Afterwards the tube may be bent in order to get the final shape.

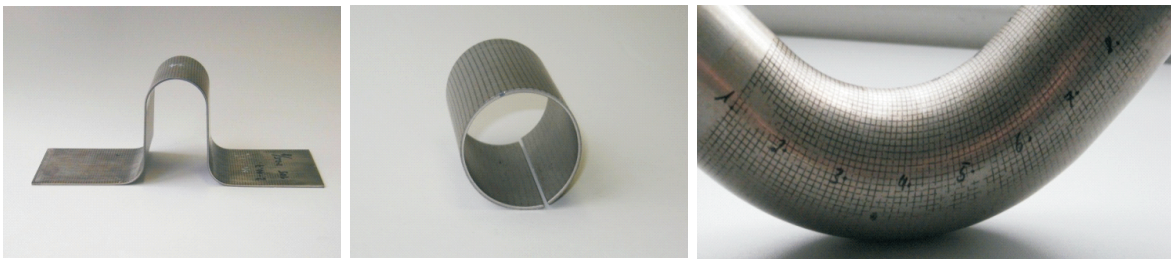

Figure 13: Forming process of a sheet to a tube

The main goal of simulation is the optimization of the structural properties of the manufactured tube with respect to very-high-cycle fatigue. Therefore, the control of the strain-induced martensite and thus an accurate computation of the martensite evolution is required. At this point we focus on the first stage of the forming-process, the U-forming . Here exist several possibilities to control the martensite evolution: Apart from the strain rate and the initial temperature one can also vary the retention force F that appears at the holders while the sheet is pressed in the given form by a special tool.

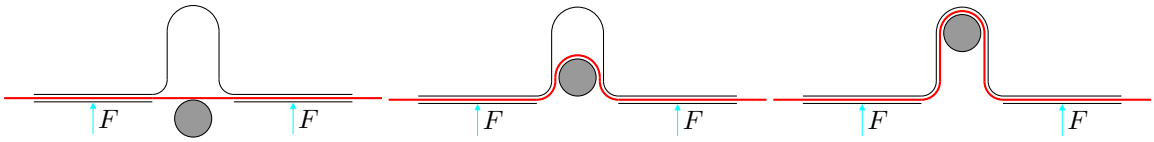

Figure 14: Schematics of the forming process presented in Figure 13

The evolution of martensite is modeled as presented in Section 3, all variables like plastic strain, temperature and martensite ratio, which are of central interest during the process, are calculated by means of a UMAT-subroutine for Abaqus. Our results are displayed in Figures 15 and 16. The martensite volume fraction is presented for retention

forces of 150kN and 210kN. We see that the amount of martensite strongly depends on the applied forces. This result is though not self-evident: On the one hand a higher force F causes ultimately much higher plastic strains and therefore leads to a support of martensite evolution. However, it also causes higher temperatures so that the formation of martensite embryos should be inhibited. During U-forming, however, it seems that the increase of ε^p after raising the retention force is so strong that it dominates the process of martensite evolution in this example.

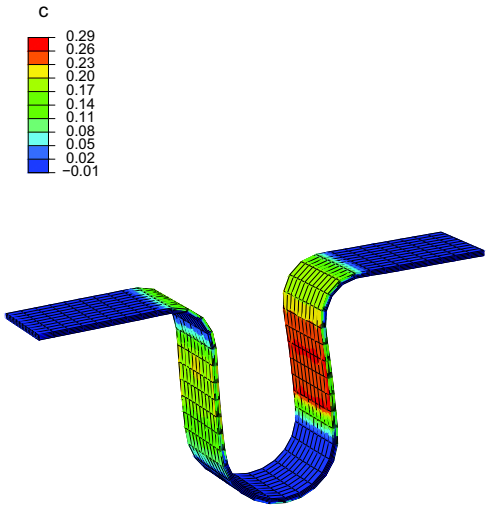

Figure 15: Martensite in the U-formed sheet, $F = 150$kN, $t_{\text{total}} = 500$s, $T(0) = 23°\text{C}$

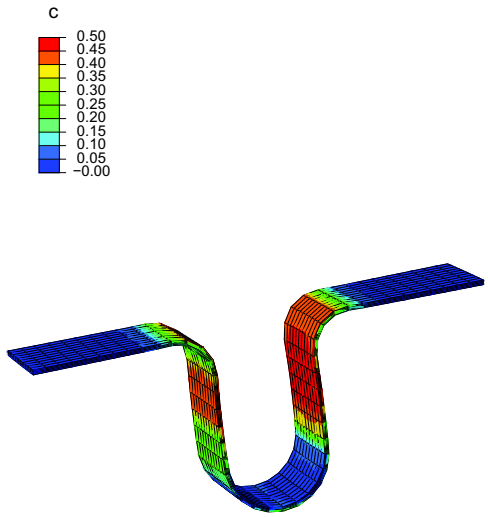

Figure 16: Martensite in the U-formed sheet, $F = 210$kN, $t_{\text{total}} = 500$s, $T(0) = 23°\text{C}$

Acknowledgements

This material is based upon work supported by the German research foundation (DFG) under Award Number SPP 1204.

References

Dally, T.; Weinberg, K.: Deformation-induced martensite formation during cold-working of metastable stainless steel. *to be submitted to: Materials Science and Engineering A*, (2011).

Dimatteo, A.; Lovicu, G.; Desanctis, M.; Valentini, R.; Solina, A.: Microstructures and properties of transformation induced plasticity steels. *Associazione Italiana di Metallurgia*, 98(11-12), (2006), 37–41.

Fischer, F. D.; Reisner, G.; Werner, E.; Tanaka, K.; Cailletaud, G.; Antretter, T.: A new view on transformation induced plasticity (trip). *International Journal of Plasticity*, 16, (2000), 723–748.

Heinemann, G.: *Virtuelle Bestimmung des Verfestigungsverhaltens von Bändern und Blechen durch verformungsinduzierte Martensitbildung bei metastabilen rostfreien Stählen*. Dissertation, ETH Zürich (2004).

Krupp, U.; Christ, H. J.: Deformation-induced martensite formation during cyclic deformation of metastable austenitic steel: Influence of temperature and carbon content. *Mater.Sci.Eng.A*, 481-482, (2008), 713–717.

Müller-Bollenhagen, C.: *Verformungsinduzierte Martensitbildung bei mehrstufiger Umformung und deren Nutzung zur Optimierung der HCF- und VHCF-Eigenschaften von austenitischem Edelstahlblech*. Dissertation, Universität Siegen (2011).

Olson, G. B.; Cohen, M.: Kinetics of strain-induced martensitic nucleation. *Metall. Trans A*, 6A, (1975), 791 – 795.

Springub, B.: *Semi-analytische Betrachtung des Tiefziehens rotationssymmetrischer Bauteile unter Berücksichtigung der Martensitevolution*. Dissertation, PZH-Verlag, Universität Hannover (2006).

Stringfellow, R. G.; Parks, D.; Olson, G. B.: A constitutive model for transformation plasticity accompanying strain-induced martensitic transformations in metastable austenitic stainless steels. *Acta Metall. Mater.*, 40, (1992), 1703–1716.

Tomita, Y.; Iwamoto, T.: Constitutive modeling of trip steel and its application to the improvement of mechanical properties. *Int. J. Mech. Sci.*, 37, (1995), 1295–1305.

Tsuta, T.; Cortes, J.: Flow stress and phase transformation analyses in austenitic stainless steel under cold working, part 2: Incremental theory under multiaxial stress state by the finite-element method. *JSME Int J.*, 36, (1993), 63–72.

Waitz, T.; Tsuchiya, K.; Antretter, T.; Fischer, F. D.: Phase transformations of nanocrystalline martensitic materials. *MRS Bulletin*, 34, (2009), 814 – 821.

Address:
M.Sc. Tim Dally and Prof. Dr.-Ing. Kerstin Weinberg, Lehrstuhl für Festkörpermechanik, Universität Siegen, D-57068 Siegen
Dr.-Ing. C. Müller-Bollenhagen and Prof. Dr.-Ing. H.-J. Christ, Lehrstuhl für Materialkunde und Werkstoffprüfung, Universität Siegen, D-57068 Siegen
email: `dally@imr.mb.uni-siegen.de; weinberg@imr.mb.uni-siegen.de`